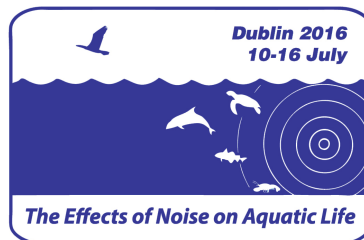




Fourth International Conference on the Effects of Noise on Aquatic Life

Dublin, Ireland
10-16 July 2016



Acoustic particle motion measurement for bioacousticians: principles and pitfalls

Michael D. Gray

Institute of Biomedical Engineering, University of Oxford, Oxford, UK; michael.gray@eng.ox.ac.uk

Peter H. Rogers

*School of Mechanical Engineering, Georgia Institute of Technology, Atlanta, GA;
peter.rogers@me.gatech.edu*

David G. Zeddies

JASCO Applied Sciences, Silver Spring, MD; david.zeddies@jasco.com

It is currently thought that all fishes detect acoustic particle motion, and it is therefore critical to measure this vector quantity when studying hearing, acoustic behavior, and noise impacts. Proper measurement of particle motion in any of its forms (acceleration, velocity, or displacement) is subject to a range of errors whose magnitude depends on the sound source(s) of interest and the environments in which they are observed. Particle motion measurement principles and errors have primarily been addressed in the literature for free field plane waves. However, such fields are rarely encountered in bioacoustic studies, and experiments or calculations made based on plane wave assumptions can lead to substantially erroneous measurement results and flawed study conclusions. This paper presents a unified treatment of underwater acoustic particle motion measurement by reviewing acoustic field attributes of commonly encountered source/environment scenarios, quantifying measurement error sources, and concluding with guidelines and recommendations for bioacoustic studies.



1. BACKGROUND AND SIGNIFICANCE

All fishes are capable of detecting acoustic particle motion (Fay, 1984), while some fishes additionally sense acoustic pressure (Popper *et al.*, 2003). Similarly, invertebrates likely sense particle motion (Mooney *et al.*, 2012), and some may have additional pressure sensitivity (Radford *et al.*, 2016). The relative contributions of pressure and particle motion to hearing may vary with species, and these contributions are not currently well understood. In hearing experiments involving fishes and invertebrates, it is therefore critical to measure or correctly predict particle motion, often in combination with pressure. While pressure is a relatively familiar and well-documented aspect of sound, particle motion is less so in the context of bioacoustic studies. Pressure is a scalar quantity and can be measured directly using a hydrophone. Particle motion is a vector quantity that requires specialized sensors or additional measurements and calculations if hydrophones are used.

Measurement of particle motion in any of its forms (acceleration, velocity, or displacement) is subject to a range of errors whose magnitude depends on the sound source(s) of interest and the environments in which they are observed. Particle motion measurement principles and errors have primarily been addressed in the literature for free field plane waves (for example, see Fahy, 1995). However, such waves are rarely encountered in practice, and experiments or calculations made based on plane wave assumptions can lead to substantially erroneous measurement results and flawed study conclusions. Here, we present a unified treatment of underwater acoustic particle motion measurement by reviewing acoustic field attributes of commonly encountered source/environment scenarios, quantifying measurement errors, and presenting guidelines and recommendations for particle motion measurement for bioacoustic studies.

2. PRESSURE AND PARTICLE MOTION FIELDS

The limitations and errors associated with particle motion measurement vary with the acoustic field (source type and boundary conditions) as well as the measurement method itself. In this section we describe the pressure and particle motion fields for four scenarios: (1) a free field plane wave, (2) the nearfield of a point source, (3) a pressure release duct below its cutoff frequency, and (4) a subsonic boundary wave.

Sound in water obeys the fluid momentum equation, here expressed by the Navier-Stokes equation for a Newtonian fluid (White, 2011):

$$\rho \left(\frac{\partial \mathbf{v}}{\partial t} + \mathbf{v} \cdot \nabla \mathbf{v} \right) = -\nabla p + \mu \nabla^2 \mathbf{v} + \rho \mathbf{g} \quad (1)$$

where ρ is the fluid density, \mathbf{v} is the particle velocity, ∇p is the pressure gradient, μ is the viscosity, and \mathbf{g} is gravity. Bold symbols indicate vector quantities. For most cases of practical interest, acoustic particle motion can be found from the lossless, linearized version of Eq. (1):

$$\mathbf{a} \sim -\frac{1}{\rho} \nabla p \quad (2)$$

where \mathbf{a} is the particle acceleration vector. Acceleration, velocity, and displacement (\mathbf{x}) are related by time derivatives:

$$\mathbf{a} = \frac{\partial \mathbf{v}}{\partial t} = \frac{\partial^2 \mathbf{x}}{\partial t^2} \quad (3)$$

In the following subsections, pressure and particle velocity are calculated using Eqs. (2) and (3) for each of the four field scenarios listed above. A frequency range between 50 and 2000 Hz is explored, as it is most relevant for a majority of fish or invertebrate hearing studies. Illustrations and example calculations for each of these fields are presented in Fig. 1.

2.1 Free Field Plane Wave

In this, the simplest of idealized cases, an unbounded planar wave front propagates without losses. Although commonly invoked for arbitrary sound field analyses, source nearfield effects and/or boundary interactions limit the likelihood of encountering free field plane wave conditions in fish bioacoustic study environments. For a plane wave propagating in the x -direction, the pressure may be written (Pierce, 1989):

$$p_{pw} = p_o e^{ik_0 x} e^{-i\omega t} \quad (4)$$

where p_o is the pressure amplitude, $k_0 = \omega/c$ is the acoustic wavenumber, ω is angular frequency, and c is the sound speed in water. The particle velocity components, derived from Eq. 2, 3, and 4, while taking $e^{-i\omega t}$ as the expression of phase change with respect to time, are:

$$v_{pw,x} = p_{pw}/\rho c; v_{pw,y} = v_{pw,z} = 0 \quad (5)$$

As seen in Fig.1B, blue lines depict pressure wave fronts (and the underlying amplitude and polarity variations in space), and the red arrows indicate the size and direction of particle velocity. All fields are shown at a single instant in time, assuming steady state conditions. The particle motion vector is parallel to the propagation direction. Figure 1C shows the magnitude ratios of the particle velocity components to $p/\rho c$. Even though there is only one non-trivial particle motion component, neither a point pressure measurement nor a single (fixed) axis motion sensor is adequate to determine the propagation axis.

2.2 Point Volume Source (Monopole)

The monopole source model describes a radiating object that is small compared to a wavelength (“acoustically small”) and whose surface vibration produces an acoustic field due to a time varying volume change. This model may be relevant for characterizing fish vocalizations or underwater transducers. Here we emphasize the nearfield of a point volume source, where the relationship between pressure and particle motion is dependent on frequency and distance from the source (r). The pressure is:

$$p_{ptsrc} = p_o \frac{e^{ik_0 r}}{r} e^{-i\omega t} \quad (6)$$

The particle velocity components are:

$$v_{ptsrc,r} = \frac{p_{ptsrc}}{\rho c} \left(1 + \frac{i}{k_0 r}\right); v_{ptsrc,\theta} = v_{ptsrc,\phi} = 0 \quad (7)$$

where the tangential components ($v_{ptsrc,\theta}$ and $v_{ptsrc,\phi}$ in spherical coordinates) are identically zero. These relations lead to the field shapes illustrated in Fig. 1E.

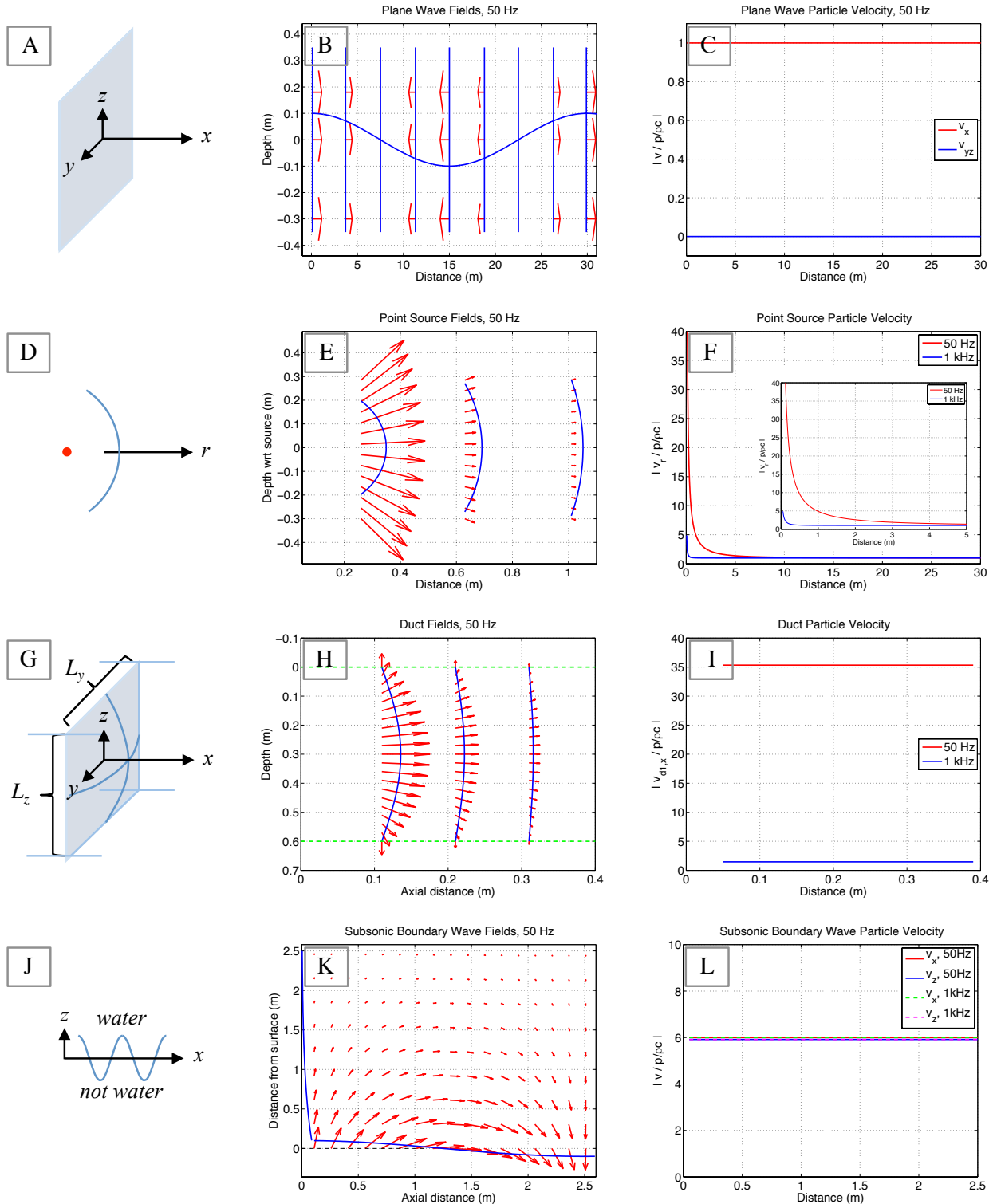


Figure 1. Illustrations (left column), pressure and particle velocity field examples (center column), and particle motion ratios (right column) for plane wave (first row), point monopole (second row), pressure release duct (third row) and subsonic boundary wave (fourth row) fields. Particle velocity directions are shown at one instant in time, but will point in the opposite direction during a half-period of the oscillation frequency.

In Eq. (7), the bracketed terms show that the radial particle velocity consists of a ‘plane wave’ contribution and a nearfield contribution. The latter is in quadrature (90° out of phase) with the former, and describes how the kinetic energy (fluid motion) is enhanced at acoustically small distances from the source (Fig. 1F).

2.3 Pressure Release Duct Below Cutoff

In this model for approximating the fields within a laboratory fish tank, elastic wall effects are omitted, and the water volume is treated as being bounded on all sides by a pressure-release boundary. This model may be applicable to commonly available tanks with glass or plastic walls whose thickness is much less than the acoustic wavelength in water, but excluding frequencies of wall bending mode resonances (Rogers *et al.*, 2016). The axial wavenumber k_{x1} corresponding to the first mode in a duct with cross section dimensions L_y and L_z is:

$$k_{x1} = \sqrt{k_o^2 - k_{y1}^2 - k_{z1}^2}, \text{ with } k_{y1} = \frac{\pi}{L_y} \text{ and } k_{z1} = \frac{\pi}{L_z} \quad (8)$$

For frequencies well below cutoff of the first mode: $f \ll f_1 = \frac{c}{2} \sqrt{1/L_y^2 + 1/L_z^2}$, the axial wavenumber is purely imaginary and contains no frequency information:

$$k_{x1} = \pi i \sqrt{\left(\frac{1}{L_y}\right)^2 + \left(\frac{1}{L_z}\right)^2} \quad (9)$$

As a result, geometry, not wavelength, determines the problem’s controlling length scale, and the axial fields decay exponentially with distance. The pressure and the particle velocity components are:

$$p_{d1} = p_o e^{-|k_{x1}|x} \sin(\pi y/L_y) \sin(\pi z/L_z) e^{-i\omega t} \quad (10)$$

$$v_{d1,x} = \frac{p_{d1}}{\rho c} \left(\frac{i|k_{x1}|}{k_o} \right); v_{d1,y} = \frac{p_{d1}}{\rho c} \left(\frac{ik_{y1}}{k_o} \right) \cot(k_{y1}y); v_{d1,z} = \frac{p_{d1}}{\rho c} \left(\frac{ik_{z1}}{k_o} \right) \cot(k_{z1}z) \quad (11)$$

As visualized in Fig.1 H, the particle motion vectors rotate from being purely axial (parallel to the duct axis) at the center of the y-z plane ($y = L_{y1}/2, z = L_{z1}/2$) to purely tangential at the duct boundaries. As with the point source case, the particle velocities are elevated relative to $p/\rho c$, but the enhancement is independent of range. This enhancement decreases as the frequency is increased closer to the first duct cutoff frequency. For the calculations shown, $L_{y1} = L_{z1} = 0.6\text{m}$, and the cutoff frequency is 1768 Hz.

2.4 Subsonic Boundary Wave

There is a bioacoustically relevant class of waves that exist between water and its boundaries, including shear and surface waves at the water/bottom interface, and bending waves in fish tank walls. When the wave propagation speed along the boundary is slow compared to the speed of sound in water, there is a characteristic behavior where the wavenumber normal to the boundary is imaginary, and the field magnitudes exponentially decay with distance from the interface.

Although limited in spatial extent, these fields can be critical in laboratory experiments where the distance between animal and boundary are practically constrained, and also may be critical for benthic animals that are in, on or close to the water column substrate.

For a subsonic wave propagating with speed c_{sbw} in the x-direction without absorptive or geometric spreading losses, the pressure and the particle velocity components are:

$$p_{sbw} = p_o e^{ik_{sbw}x} e^{-|k_z|z} e^{-i\omega t} \quad (12)$$

$$v_{sbw,x} = \frac{p_{sbw}}{\rho c} \left(\frac{k_{sbw}}{k_o} \right); v_{sbw,z} = \frac{p_{sbw}}{\rho c} \left(\frac{i|k_z|}{k_o} \right) \quad (13)$$

where the wavenumber normal to the interface is $k_z = \sqrt{k_o^2 - k_{sbw}^2} \sim ik_{sbw}$ when $\left(\frac{c_{sbw}}{c}\right) \ll 1$. The particle motion field exhibits a characteristic circulation pattern (Fig. 1K) owing to the quadrature phase relationship between in-plane and out-of-plane components. In the examples shown, $c_{sbw} = 250$ m/s (no dispersion), and the particle velocity enhancement relative to $p/\rho c$ is simply the ratio of water and boundary wave speeds.

The particle velocity magnitude is always enhanced relative to $p/\rho c$ for the point source nearfield, duct and boundary wave cases. However, there is another important case to consider – that of the sum of an incident and reflected acoustic wave from a boundary. For example, for a source near the water surface, the ratio of vertical particle velocity to $p/\rho c$ can vary between zero and infinity as a function of frequency for a fixed depth. Together, these cases illustrate how misleading particle motion estimates can be when based on point pressure measurements.

2. PRESSURE GRADIENT SENSORS

Pressure gradient, and therefore particle motion, may be determined from the difference of two pressure measurements made at different locations in space. In practice this is done either with a pair of hydrophones with a fixed spacing (Δ) or a single hydrophone undergoing a prescribed translation. From Eqs. (2) and (3), the particle velocity component along a line connecting two pressure measurements as determined from an explicit gradient takes the form:

$$v_{\Delta p}(x, \omega) = \frac{i}{\rho c k_o} \frac{(p(x+\frac{\Delta}{2}, \omega) - p(x-\frac{\Delta}{2}, \omega))}{\Delta}; v_{\Delta p}(x, t) = \frac{1}{\rho} \int \frac{(p(x+\frac{\Delta}{2}, t) - p(x-\frac{\Delta}{2}, t))}{\Delta} dt \quad (14)$$

in the frequency and time domains, respectively. Multiple hydrophones (or 3D scanning) can be used to estimate the full particle motion vector. It is critical in calculating explicit gradients that the phase of the pressure signal not be discarded. Magnitude metrics such as root-mean-squared pressure must not be used, as they would miss gradient contributions from phase that occur in many field types. There are a variety of additional error sources arising in explicit pressure gradient measurements, including:

- spacing
- spacing uncertainty
- calibration uncertainty
- noise
- flow; and
- hydrophone acceleration sensitivity

In this section we focus on the first four error sources, and discuss the others in Section 4. For all cases, the influence of errors on particle motion estimation is quantified by the ratio of the sensor-based estimate and the actual fluid motion in the absence of any sensors.

A suitable starting point in defining a pressure gradient measurement configuration is to determine an appropriate pressure sensor spacing. The influence of spacing is shown in Fig. 2A and B for frequencies of 50 and 1000 Hz, respectively. The calculations were made using Eq. (14) as applied to the field pressure expressions in the previous section. At 50 Hz, the only significant errors over the range of spacings (Δ) shown are for the pressure release duct, where the true gradient varies rapidly in space relative to acoustic scales. At 1 kHz, growing errors are seen in all measurements as the spacing becomes larger with respect to the wavelength. Since the surface boundary wave (sbw) in these examples was modeled with a phase speed of 250 m/s, the errors increase quickly as the pressure measurement spacing approaches the sbw wavelength, shown as a vertical dashed black line. This illustrates the fact that the hydrophone spacing must be chosen to be much less than the smallest spatial scale of any wavefield (e.g. with the largest wavenumber k_{max}) that may be encountered in the bioacoustic measurement scenario under study: $k_{max}\Delta \ll 1$.

Figures 2C and D show errors induced by a separation uncertainty of 2 and 4 mm, respectively. The effects of these uncertainties are only significant at the smallest values of Δ . Therefore, gradient measurements appear to be tolerant of positioning uncertainties that may be encountered in realistic measurement rigging scenarios.

In contrast, the effect of a small uncorrected calibration magnitude bias in one of the two pressure measurements (e.g. one of two hydrophones) is seen in Fig. 2E and F to be profound. Results are shown for biases of 5 and 10%. These correspond to having one phone whose calibration is perfect, and the other whose calibration is inaccurate by +0.42 or +0.83 dB, respectively, yet the impact of a calibration bias is both strong and complex. As an example, for plane waves the calibration bias introduces an artificial magnitude component to the measured gradient, which physically is purely due to phase. Since this phase difference is small at low frequencies, a seemingly small calibration uncertainty introduces an enormous particle motion overestimate. At high frequencies, the gradient from phase is large, so the calibration uncertainty error is only apparent at small separations (where $k_x\Delta$ is still fairly small). These results highlight the somewhat counterintuitive result that low frequency plane wave measurements can place stringent demands on calibration accuracy. Moreover, typical factory calibration uncertainties are sufficient to ruin a gradient measurement in several common measurement scenarios. Although not quantified here, it is further noted that hydrophone phase response uncertainties may further degrade estimates of particle motion: calibration of both magnitude and phase is important.

In a realistic experiment, both spacing and calibration uncertainties will be present. The cumulative effects of these uncertainties are shown in Fig. 3 as a function of frequency, here parameterized as the nominal spacing Δ normalized by acoustic wavelength λ_0 . In these examples, fixed spacings of 20 and 40 cm were chosen to illustrate the problems in trying to make broadband measurements with gradient sensors. Many of the trends are as seen in the previous figures. The feature above $\Delta/\lambda_0 = 0.2$ in the duct case occurs as the axial wavenumber becomes real-valued above the first mode cutoff. These results suggest that explicit gradient measurements made within the modest error bounds described here are not well suited for data collection over a broad frequency band. We further note that while all errors have been quantified in terms of velocity ratio magnitudes, there are corresponding motion phase errors, which may degrade estimates of the direction of a sound source (Section 4.1).

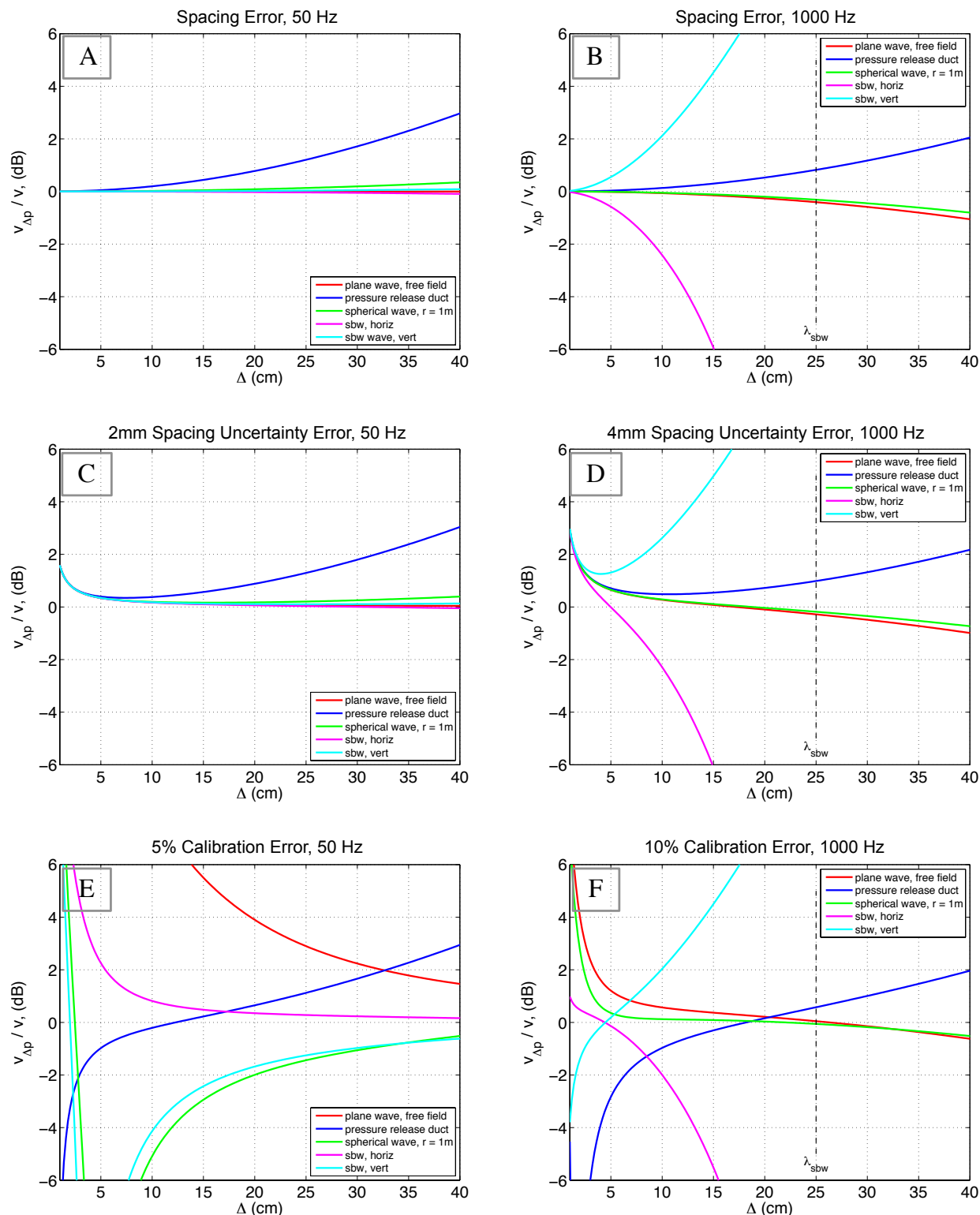


Figure 2. Explicit pressure gradient errors associated with absolute spacing (top row), spacing uncertainty (middle row), and calibration uncertainty (bottom row), for frequencies of 50 Hz (left column) and 1kHz (right column). SBW horiz and vert refer to the motion components of the surface boundary wave along the boundary and into the water column, respectively.

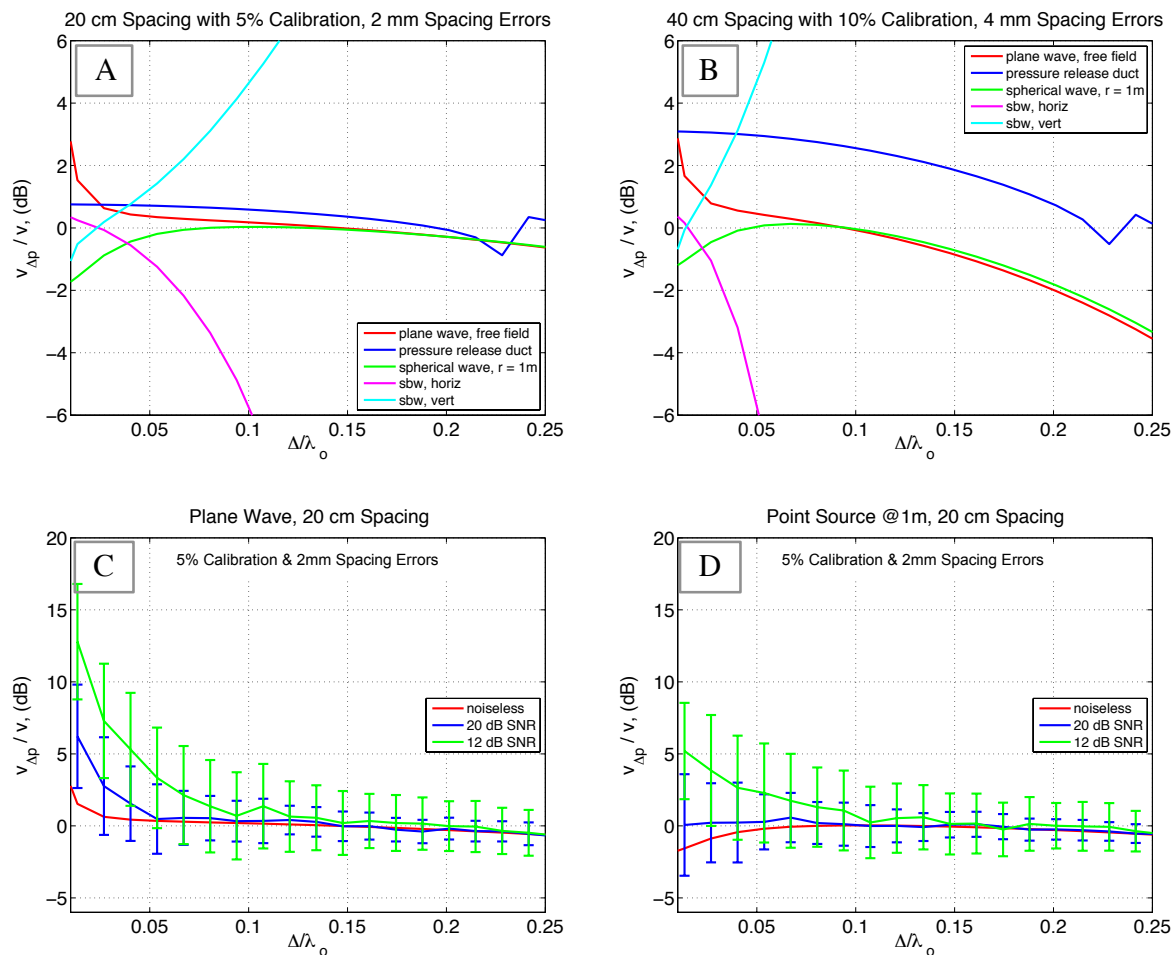


Figure 3. Cumulative pressure gradient errors due to spacing and calibration uncertainties, and noise. (A) 20cm spacing, 5% calibration and 2mm spacing errors, noiseless, (B) 40cm spacing, 10% calibration and 4mm spacing errors, noiseless, (C) plane wave field with 20cm spacing, 5% calibration and 2mm spacing errors, 12 and 20 dB SNR, (D) point source field with 20cm spacing, 5% calibration and 2mm spacing errors, 12 and 20 dB SNR. In (C) and (D), error bars indicate ± 1 standard deviation over 100 ensembles of random noise.

Finally, the effect of noise on the gradient calculation is shown for the case of incoherent noise added to the constituent pressure measurements in plane wave (Fig. 3C) and point source fields (Fig. 3D) for individual pressure signal to noise ratios (SNRs) of 20 and 12 dB. Results are shown for the mean and ± 1 standard deviation of 100 random noise realizations. The calculation is most noise-sensitive when the gradient is smallest – at low frequencies in plane wave fields.

3. INERTIAL MOTION SENSORS

Direct underwater particle motion measurements can be made using sensors whose output is determined by relative motion of a reference mass and the sensor casing. These are commonly available as accelerometers or geophones, operated below and above their primary resonances, respectively. Since most of these devices are not built for submerged environments, some modifications are typically required. The list of technical issues for inertial motion sensor use for underwater particle motion measurements include the following, the first three of which are addressed in this section:

- buoyancy
- geometry (size and shape)
- compliance
- suspension, and
- flow

As a matter of metrology, it is good practice to not change the field being measured in the process of making the measurement. Although many natural hearing systems do not follow this tenet, the objective of acoustic field characterization is to provide a reference field that would be present in the absence of a sensor or the animal being studied. In making an underwater sensor minimally invasive to the acoustic environment, the buoyancy of the sensor package (including cabling) is a primary consideration. Specifically, the dynamic (moving) mass of the sensor should be equal to that of the water displaced by the sensor. With accelerometers (operating below resonance), all sensor components are moving, so that the static and dynamic masses are equal, and buoyancy can be qualitatively assessed by submerging the sensor and observing its displacement. With geophones (operating above resonance), the internal reference mass is stationary, so determination of in-water dynamic buoyancy requires additional information from the manufacturer.

The effects of sensor buoyancy and size, along with many other practical aspects of underwater particle motion sensor design, have been described for a rigid sphere in a plane acoustic wave field (Leslie *et al.*, 1956). Example results are shown in Fig. 3A for sensor of diameter $d=20\text{cm}$ and specific gravity (sg) values of 1.20, 1.00 and 0.83. Responses are quantified by the magnitude ratio of the sensor motion in the direction of propagation (v_s), normalized by the fluid motion in the absence of the sensor (v_{inc}). At low frequencies ($d/\lambda_0 \ll 1$), the rigid, spherical neutrally buoyant sensor ($sg = 1.00$) is predicted to move as the fluid would in the absence of the sensor. For non-unity specific gravities, the low frequency responses amount to a modest calibration offset. As frequency increases, all responses decrease in magnitude as a consequence of the spatial integration of the acoustic field over the sensor body. That is, the acoustic size of the sensor acts as a low pass filter. This effect is not always detrimental, as it can be useful in reducing the impact of high wavenumber noise (e.g. from flow), as will be discussed in the next section.

Real sensors and their enclosures have finite impedances (compliance > 0), and the sensor shape need not be spherical. To examine these and other effects in combination, finite element model calculations of elastic sensor enclosure responses were made using axisymmetric and 3D formulations in PZFlex (Weidlinger Associates Inc., Cupertino, CA). Mesh convergence was confirmed by reducing the element size in increments of no less than 20% until the particle motion results changed less than 1% at the highest frequency.

Fig. 4B compares the responses of a sphere and unity aspect ratio cylinder both with longitudinal and shear speeds of steel ($c_L = 5900$, $c_s = 3200$ m/s), to that of a rigid sphere, all with unity specific gravity and 20 cm diameter. The sphere results track each other closely, while the cylinder shows a stronger attenuation with increasing frequency. This shows the importance of shape with regard to the spatial integration of pressure forces in the direction of propagation: forces acting on the sphere have diminishing contributions near $\pm d/2$ due to the vanishing polar surface area, while the forces on the cylinder are concentrated at $\pm d/2$. Therefore, the cylinder appears to be acoustically larger. If the cylinder were rotated so that the flat ends were orthogonal to the propagation direction, its response would be close to that of the sphere.

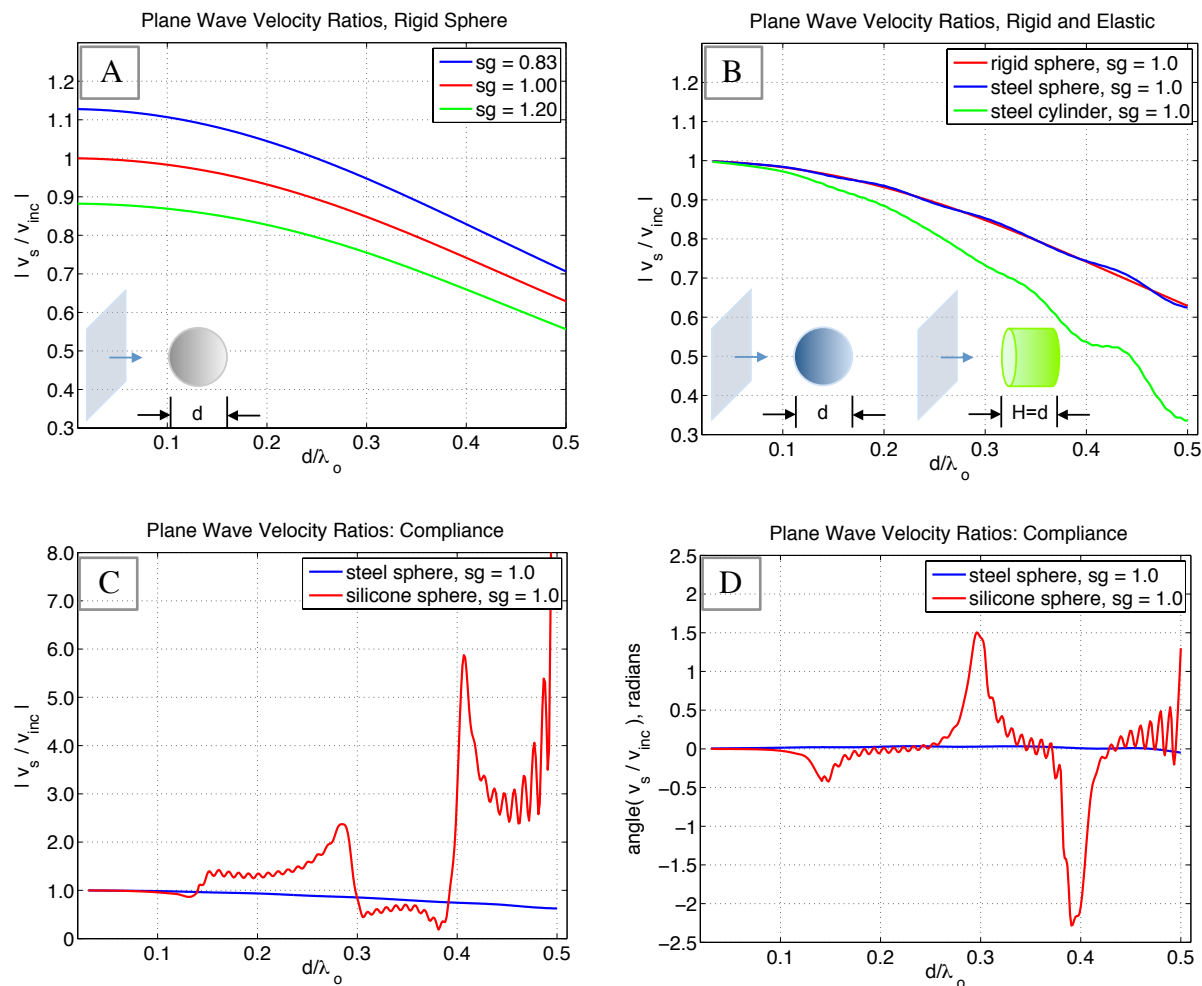


Figure 4. Plane wave responses of solid sensor body models: (A) analytical solution for rigid sphere response magnitude with varying specific gravities, (B) neutrally buoyant rigid sphere, elastic sphere, and elastic cylinder response magnitudes, (C) neutrally buoyant steel and silicone sphere response magnitude and (D) phase.

In the examples presented thus far, the compliance of the sensor body has been kept to a minimum. Fig. 4C and D compare the magnitude and phase responses of a neutrally buoyant sphere with silicone-like wave speeds ($c_L = 1100$, $c_s = 200$ m/s) to the response of the steel-based sphere from Fig. 4B. The silicone sphere exhibits a series of resonances that cause significant deviation from the ideal response starting near $d/\lambda_o \sim 0.1$. Application of even more compliant materials (e.g. closed cell foam) would push the resonances even lower in frequency for a fixed material thickness. These results reinforce the notion that enclosures for underwater sensors must have minimal compliance in order to minimize measurement errors and field disturbance.

To examine how a sensor body may respond to subsonic surface waves such as those described in Section 2, models were run in order to calculate particle velocities near a line-driven interface between water and sediment-like ($c_L = 1500$ m/s, $c_s = 250$ m/s, $sg = 1.05$) half spaces, illustrated in Fig. 5A. As with the previous finite element calculations, the sensor body was a sphere with 20 cm diameter, unity specific gravity, and wave speeds of steel. The sphere was placed 0.25 m above the interface and 2.25 m away from the drive location, so that the slow and

fast waves emanating from the drive location could be temporally separated and analyzed. As seen in Fig. 5B, the sensor body motion is heavily attenuated in a subsonic wave field, relative to a plane acoustic (water) field in the same frequency range. The oscillations in the low frequency response are primarily caused by interference between shear and interface wave arrivals at slightly different times. Spatial integration by the elastic sensor body changes how waves with different propagation speeds interact at the observation location. These results reiterate that motion sensors must be small compared to the shortest wave field length scale that may be encountered, and this may be much smaller than the acoustic wavelength.

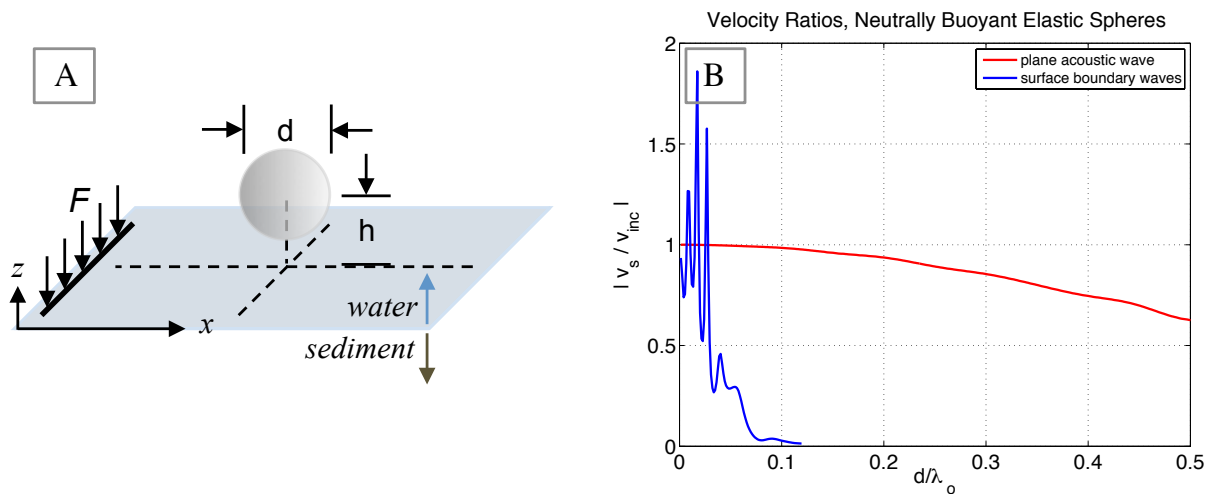


Figure 5. Response of a spherical sensor body $h=0.25m$ above the interface between line-driven water and soft-sediment half spaces: (A) model illustration and (B) response magnitudes as a function of sensor diameter normalized by acoustic wavelength.

4. OTHER CONSIDERATIONS

There are several other considerations for underwater particle motion sensing beyond those discussed above. Here we highlight the most critical of these issues and provide references for further study by the interested reader.

4.1 Acoustic Intensity Measurement

For most bioacoustics studies the polarities of the pressure and particle motion signals are irrelevant: acoustic sensitivities to p and $-p$, and v and $-v$, are the same. However, time-averaged intensity, which is key to determining the direction to a sound source and for resolving the 180° ambiguity, depends on the polarity of both pressure and particle velocity. The time averaged radial intensity is a non-oscillatory quantity equal to the time average of the product of the pressure and radial particle velocity: $I_r(t) = \langle p(t) \cdot v_r(t) \rangle$. In the complex frequency domain it is equal to the real part of the product of the complex amplitude pressure and complex conjugate of the amplitude of the complex radial particle velocity: $I_r(\omega) = \text{real}(p(\omega) \cdot \text{conj}(v_r(\omega)))$. The sign of the radial intensity determines whether a fish that is oriented to the particle velocity is facing towards or away from the source. Obtaining the correct sign of the intensity is trickier than it might at first seem:

1. For many commercially available hydrophones, a positive output voltage corresponds to a negative acoustic pressure, but polarity is often not documented by the manufacturer.

2. For the output of an accelerometer to be proportional to $+v_r$, an accelerometer must be pointed away from the source, although the axis of “positive” response is not always documented by the manufacturer.
3. For both measurements, inadvertent polarity inversions in system cabling or the data acquisition instrumentation must be avoided.
4. Proper conversion from acceleration to velocity in the frequency domain requires knowledge of the time dependence sign convention (e.g. $e^{+i\omega t}$ or $e^{-i\omega t}$). We note that Matlab (Mathworks, Natick, MA) employs $e^{+i\omega t}$.
5. To obtain the correct relative phase, which is essential when $\text{Re}(pv_r^*)$ is used to obtain the time averaged intensity, any signal conditioning done for the pressure must also be done for the particle motion.

4.2 Flow Noise

Water flow is known to adversely impact the performance of both pressure gradient and inertial underwater sensors (Finger *et al.*, 1979; Lauchle *et al.*, 1996) through the generation of noise by pressure fluctuations with characteristic length scales on the same order as the sensor itself (and much smaller than an acoustic wavelength). Flow noise alleviation methods include the use screens to reduce the flow at the sensor (Keller, 1977), use of sensor size to increase spatial integration (Martin and Leehey, 1977), separation of the sensor from the surrounding flow using a lossy elastomer (Ko and Schloemer, 1992), and signal processing in combination with pressure measurements (Korenbaum and Tagiltsev, 2012). Choice of enclosure shape has also been shown to strongly influence flow noise generation on bluff bodies (McEachern and Lauchle, 1995).

4.3 Sensor Suspension

Even in the absence of flow, the method of sensor suspension can greatly influence the performance of a particle motion sensor. As discussed by Kim (2004), the suspension should fix the position and orientation of the sensor without inhibiting its movement or introducing measurement errors. Several examples of suspension methods have been demonstrated, including spring-mounted (Leslie *et al.*, 1956), elastically-constrained (Gabrielson *et al.*, 1994) and compliantly-suspended sensors (McConnell, 2002).

4.4 Internal Complexity

The sensor body models presented in this paper were simplified to show effects of bulk properties in a variety of field types. However, the mounting of internal masses inside a container has been shown to decrease the expected bandwidth (Leslie *et al.*, 1956; Gabrielson *et al.*, 1994). It is important therefore to determine the full mounted and suspended response of an enclosed motion sensor during experiment planning.

4.5 Spurious Coupling

All real transducers will respond at some level to signals not ideally sensed by a given sensor type. Hydrophones, even if carefully built, may exhibit high sensitivity to acceleration (Bruel & Kjaer), with enhanced error susceptibility in fields with high kinetic to potential energy ratios (Surry *et al.*, 1996). Motion sensors have varying degrees of cross-axis sensitivity, such that fluid motion purely orthogonal to the sensing axis will still generate an output. Many manufacturers

have ratings for these quantities, but they are best calibrated in a well-defined acoustic field after a candidate sensor system has been fully assembled in its deployment rigging.

5. CONCLUSIONS AND RECOMMENDATIONS

It is clear from the results presented here that plane wave analyses are not adequate to describe sensor behaviors in many relevant bioacoustic measurement scenarios. In particular, the relation ($v=p/\rho c$) is rarely of value except under true plane wave conditions, as it typically misinforms about the magnitude of the particle velocity and provides no information about direction.

Gradient measurements appear to be best suited to controlled laboratory environments where the impact of calibration uncertainties can be mitigated or eliminated by scanning a pressure field with a precision positioner, and where the effects of incoherent noise can be minimized with ambient noise control measures and/or coherent averaging, if applicable.

Inertial motion sensors, when enclosed in a low-compliance package, appear to be relatively fault tolerant, although several practical deployment issues must also be addressed for deployment.

All enclosures will have resonances no matter how rigidly constructed, so it is important to determine the full useful bandwidth of candidate devices and weigh this information against the desired bioacoustics measurement frequency range.

Whether using inertial or explicit gradient sensors, the largest dimension of the overall device should be kept smaller than a tenth of the shortest wavelength of interest, which is not necessarily acoustic (λ_0). For experiments in laboratory tanks, preliminary vibration measurements on the walls may be needed to determine the flexural wave speed. If experiments near the bottom of the water column are of interest, preliminary core sample characterization or bottom mounted geophone measurements may be valuable in determining the speeds and propagation ranges of subsonic waves.

Best practices in sensor design and deployment can be counteracted by omission of important information during data processing. Care should be taken to keep track of sensor polarities, particle motion sensor orientation, and Fourier transform conventions for frequency domain calculations.

Despite growing interest in underwater motion sensing for bioacoustics, there is a dearth of readily available and reliable sensor options. Further efforts are needed to develop such sensors, and it is hoped that the results and references in this paper assist in this endeavor.

ACKNOWLEDGEMENTS

The authors wish to acknowledge Art Popper, Dick Fay, James Martin, Jayme Caspall, and Nathan Martin for helpful discussions over the last 25 years, and Constantin Coussios for access to computational resources.

REFERENCES

- Brueel & Kjaer Product data sheet for hydrophones 8103, 8104, 8105 and 8106.
- Finger, R.A., Abbagnaro, L.A., and Bauer, B.B. (1979), "Measurements of low-velocity flow noise on pressure gradient hydrophones," *J. Acoust. Soc. Am.* **65**(6), 1407-1412.
- Fahy, F. (1995), *Sound Intensity 2nd Edition*, (E & FN Spon, London), 114-117.
- Fay, R. R. (1984), "The goldfish ear codes the axis of acoustic particle motion in three dimensions," *Science*, **225**(4665), 951-954.
- Gabrielson, T.A., Gardner, D.L., and Garrett, S.L. (1994), "A simple neutrally buoyant sensor for direct measurement of particle velocity and intensity in water," *J. Acoust. Soc. Am.* **97**(4), 2227-2237.

- Kim, K., Gabrielson, T.B., and Lauchle, G.C. (2004), "Development of an accelerometer-based underwater intensity sensor," J. Acoust. Soc. Am. **116**(6), 3384-3392.
- Keller, B.D. (1977), "Gradient hydrophone flow noise," J. Acoust. Soc. Am. **82**(1), 205-208.
- Ko, S.H., and Schloemer, H.H. (1992), "Flow noise reduction techniques for a planar array of hydrophones," J. Acoust. Soc. Am. **92**, 3409-3424.
- Korenbaum, V.I. and Tagiltsev, A.A. (2012), "Flow noise of an underwater vector sensor embedded in a towed array," J. Acoust. Soc. Am. **131**(5), 3755-3762.
- Lauchle, G.C., McEachern, J.F., Jones, A.R., and McConnell, J.A. (1996), "Flow induced noise on pressure gradient hydrophones," AIP conference proceedings **368**, 202-225.
- Leslie, C.B., Kendall, J.M., and Jones, J.L. (1956), "Hydrophone for measuring particle velocity," J. Acoust. Soc. Am. **28**(4), 711-715.
- Martin, N.C., and Leehey, P. (1977), "Low wavenumber wall pressure measurements using a rectangular membrane as a spatial filter," J. Sound and Vibration **52**(1), 95-120.
- McConnell, J.A. (2003), "Analysis of a compliantly suspended acoustic velocity sensor," J. Acoust. Soc. Am. **113**(3), 1395-1405.
- McEachern, J. F., and Lauchle, G. C. (1995), "Flow-induced noise on a bluff body," J. Acoust. Soc. Am. **97**, 947-953.
- Mooney, T. A., Hanlon, R., Madsen, P. T., Christensen-Dalsgaard, J., Ketten, D. R., & Nachtigall, P. E. (2012). "Potential for sound sensitivity in cephalopods." in *The Effects of Noise on Aquatic Life* (Springer, New York), pp. 125-128.
- Pierce, A. (1989), *Acoustics, an introduction to its physical principles and applications*, (Acoustical Society of America, Woodbury, NY).
- Popper, A. N., Fay, R. R., Platt, C., & Sand, O. (2003). "Sound detection mechanisms and capabilities of teleost fishes," in *Sensory processing in aquatic environments* (Springer New York), pp. 3-38.
- Radford, C., Tay, K., and Gueritz, M. (2016), "Hearing in the paddle crab *Ovalipes catherus*," presented at the 4th International Conference on the Effects of Noise on Aquatic Life.
- Rogers, P., Hawkins, A., Popper, A., Fay, R., & Gray, M. (2016). "Parvulescu revisited: tank acoustics for bioacousticians," in *The Effects of Noise on Aquatic Life II*, edited by N. A. Popper, and A. Hawkins (Springer New York, New York, NY), 933-941
- Surry, J., Kezele, D., and Risley, C. (1996), "The contamination of acoustic pressure measurements by sensor oscillations," AIP conference proceedings **368**, 226-247.
- White, F.M. (2011), *Fluid mechanics, 7th edition* (McGraw-Hill, New York).